J. Appl. Comput. Mech., 7(3) (2021) 1383-1402
DOI: 10.22055/JACM.2020.32143.1975

ISSN: 2383-4536
jacm.scu.ac.ir

Shahid Chamran University of Ahvaz

Journal of Applied and Computational Mechanics

Research Paper

Comparative Study of Mixed Convective MHD Cu-Water Nanofluid Flow over a Cone and Wedge using Modified Buongiorno's Model in Presence of Thermal Radiation and Chemical Reaction via Cattaneo-Christov Double Diffusion Model

Sawan Kumar Rawat, Himanshu Upreti, Manoj Kumar

Department of Mathematics, Statistics and Computer Science, G.B. Pant University of Agriculture and Technology, Pantnagar, Uttarakhand, India

Received January 03 2020; Revised February 13 2020; Accepted for publication March 03 2020.
Corresponding author: S.K. Rawat (sawan.rawat@gmail.com)

Abstract. The steady Cu-water nanofluid flow in presence of magnetic field is investigated numerically under the effects of mixed convection, thermal radiation and chemical reaction. For investigating the nanofluid flow, the flow over two different geometries, cone and wedge have been considered. The Tiwari and Das nanofluid model is implemented together with Buongiorno nanofluid model. Thermal and concentration diffusion are studied using the Cattaneo-Christov double diffusion model. At the boundary of the surface, no slip and zero mass flux condition are implemented to control the nanoparticle volume fraction at surface. Constitutive laws of flow are obtained in form of ordinary differential equations by the use of similarity transformation. The modeled flow problem is solved numerically by the Runge-Kutta-Fehlberg method and shooting scheme. Variation in flow properties due to parameters involved is presented graphically and through tabular values. The effect of thermal radiation and thermal relaxation parameter is to increase heat transfer. The temperature of nanofluid and drag force at surface increases due to enhanced magnetic field. The nanoparticles are found to be concentrated near the surface of cone and wedge but concentration decreases with chemical reaction parameter and Schmidt number as fluid moves towards far field.

Keywords: Cattaneo-Christov model; Thermal Radiation; Chemical Reaction; Mixed Convection; Zero Wall Mass Flux.

1. Introduction

Heat transfer phenomenon occurs in many known process. Heat transfer is witnessed in the environment or medium due to the presence of temperature variation between two diverse entities or when single entity experiences variation in temperature within different parts of its body. The monotonically increasing demands in various industrial domain can be fulfilled only if new technologies witness an improvement in heat transfer performance. Present generation is witnessing increase in large sized machine in various industries like chemical or fertilizers producing industries and power stations for modern applications. But the industries are also struggling with thermal systems and to maintain their reduced size. As the conventional fluid have limited thermal characteristics, it makes them unsuitable to act as coolant for industrial purpose.

Choi [1] broke many barriers in this field when he gave the idea of suspending the nanoparticles in the traditional base fluid. With this experiment, an enhancement in thermal conductivity was witnessed. His research included many experiments validating the boosted thermal performance of nanofluid, which was later also confirmed by many other researchers and scientists. Later, many authors (see [2-9]) studied and analyzed the nanofluid flow and discussed their heat transfer performance. The aforementioned studies [2-9], analyze and discuss the flow of nanofluid over/past

Published online: March 08 2020

geometries of different shapes. However, these studies analyzed the heat transfer in accordance with law given by Fourier [10]. Fourier's law signifies the parabolic nature of energy equation and confers that heat transfer takes place with zero time lag. Cattaneo [11] pointed out the fact that heat transfer take place with a time lag. His study discussed this fact and he added factor in existing Fourier model, which was physically related to time lag. Later, Christov [12] included Oldroyd's upper convected derivatives to give his principle for material invariance. Upadhya *et al.* [13] utilized Cattaneo-Christov heat flux model to analyze the nano and micro fluid. Alamri *et al.* [14] studied second grade fluid with Cattaneo-Christov theory. They presented the fluid problem with magnetic effects and also discussed the mass transfer. Recently, some more authors (for instance see [15-18]) have also implemented the Cattaneo-Christov heat flux model to explore heat transfer characteristic.

Heat exchangers, power and solar technology, nuclear reactors etc. witness the significant amount of thermal radiation. Thermal radiation accounts to a process when a heated object emits electromagnetic radiation in every direction through unoccupied gap. Most of the objects have this property. The heat transfer through thermal radiation do not essentially require source of heat and object subjected to heat to have any contact between them. Therefore, it is an important factor to look upto while discussing the flow problems. A case of thermal radiative nanofluid unsteady flow was presented by Mabood and Khan [19], who solved the flow problem using HAM. Sheikholeslami *et al.* [20] presented a study of fluid flow by the means of two phase model. They investigated the flow under the influence of thermal radiation and analyzed the heat transfer process. Pal *et al.* [21] investigated the stagnation point flow of nanofluid over a stretching/shrinking sheet and presented the results of heat transfer in presence of non-linear thermal radiation. Many have used thermal radiation together with Cattaneo-Christov model (C-C model) to exploit the heat transfer characteristics in various fluid flow problems. One such instance is study presented by Upadhya *et al.* [13]. They investigated a steady flow, where base fluid was rich in graphene nanoparticles and dust (in micron) was also suspended. With the findings of their study, they concluded that dust phase had lower temperature in comparison to nanofluid phase. Some existing studies [22, 23] have mentioned that the devices show enhanced thermal efficiency when exposed to high temperature.

The magnetic field and chemical reaction effects are also known to alter the pace of flow and heat transport. Their applications in industrial, medical and natural fields are vast. Their presence is also known to alter the behavior of flow at boundary layer. Therefore, introducing these effects in the study of fluid flow makes it more interesting and realistic. Zangooee *et al.* [24] analyzed the MHD nanofluid flow between two rotating disks, which were stretchable in nature. The base fluid (water) was rich in titanium dioxide and Gallic oxide nanoparticles. To exploit the nature of heat transport, they analyzed the flow with Joule and radiative heating. Aleem *et al.* [25] also studied the MHD nanofluid flow through an accelerating vertical plate whose height tends to infinity. They also implemented the effects of chemical reaction and Newtonian heating. In their study, they considered the five different types of nanoparticles with water as a base fluid. Krishna and Chamkha [26] also solved the MHD nanofluid flow problem. The nanofluid was flowing past a permeable plate which was in motion. They used Perturbation method for solving the problem and also discussed the Nusselt and Sherwood number. Some others who have recently discussed the magnetic effects in nanofluid flow are Gholinia *et al.* [27], Souayeh *et al.* [28], Singh *et al.* [29], Singh *et al.* [30] and Upreti *et al.* [31]. An unsteady nanofluid flow over an infinite plate under convective boundary conditions in a binary chemical mixture was discussed by Dhlamini *et al.* [32]. They emphasized on heat transfer and mass transfer through Buongiorno's model and activation energy effect. Rasool and Zhang [33] studied Powell-Eyring nanofluid flow past a Riga plate with chemical reaction effects. Using HAM they provided the solution profiles and also discussed heat and mass transfer coefficient via tabular values. The solution to Prandtl-Eyring chemically reactive nanofluid flow problem with entropy generation was given by Khan *et al.* [34]. Khan *et al.* [35] and Yadav *et al.* [36] were others who recently looked upon the effects of chemical reaction in flow of nanofluid through different geometries.

Presently, the two mathematical models (homogeneous and non-homogeneous) are used to discuss the nanofluid transport. Homogeneous model, presented by Tiwari and Das [37] pointed out that enhanced thermophysical properties of base fluid are due to suspended nanoparticles. Buongiorno [38], who proposed the non-homogeneous model, identified seven possible factors which contribute to enhance heat transfer in nanofluid but mainly two of them, Brownian motion and thermophoresis were found to contribute significantly. Previously published literature can be found using these two models for nanofluid flow problem. Many have utilized both models in their study. Some (for instance see [39] and [40]) called it combination of Buongiorno and Tiwari and Das model whereas others (for instance see [41], [42] and [43]) have referred it as modified Buongiorno model.

In flow problems, some study the fluid flow past (or over) a geometry or in other cases the fluid motion is generated when an object of particular geometry moves through the fluid generating motion in fluid. Moreover, many aforementioned studies have focused on different geometries while dealing with flow problems. The geometry over which fluid flow plays an important role, like in designing the heat exchangers, for transpiration and fiber coating. Keeping in mind the above discussed literature, various flow effects and models of nanofluid, we have developed a mathematical model discussing the mixed convective MHD nanofluid flow with chemical reaction and thermal radiation effects over cone and wedge. Buongiorno model together with Cattaneo-Christov double diffusion model (refer to [44-49]) is used to study thermal and concentration diffusion. Also, we have utilized the correlations that defines the relationship between thermophysical properties of nanofluid with those of base fluid and volume fraction of nanoparticle, in the view of Tiwari and Das model. We have referred it as modified Buongiorno's model in this study. At the boundary, no slip condition with zero mass flux (see [7], [32], [50], [51], [52], [53], [54] etc.) is used. Local similar

equations representing the modeled problem are solved numerically. Such solutions for various boundary layer flow problems have been explored in past studies (see [7], [31], etc.) also. These kind of solutions are very useful, as they help one to examine the effect of pertinent parameters at static location from the surface. The expressions of drag coefficient and heat transfer coefficient are also discussed. Effects are analyzed and discussed via tables and graphs.

2. Description of mathematical problem

2.1 Analysis and theory of flow

Consider a two dimensional, steady, incompressible and mixed convective Cu-water nanofluid flow. Nanofluid flow is considered over vertical cone and wedge. As depicted in Fig. 1, here x axis is taken along the cone or wedge surface and y is axis normal to its surface. Magnetic field is applied perpendicular to the surface. The half angle of the cone or wedge is α and radius of cone is denoted by r. The temperature near the wall is considered as $T_w = T_\infty + ax^s$, where s stands for wall temperature related parameter and a is constant. The ambient fluid temperature and nanoparticle concentration are denoted by T_∞ and C_∞, respectively.

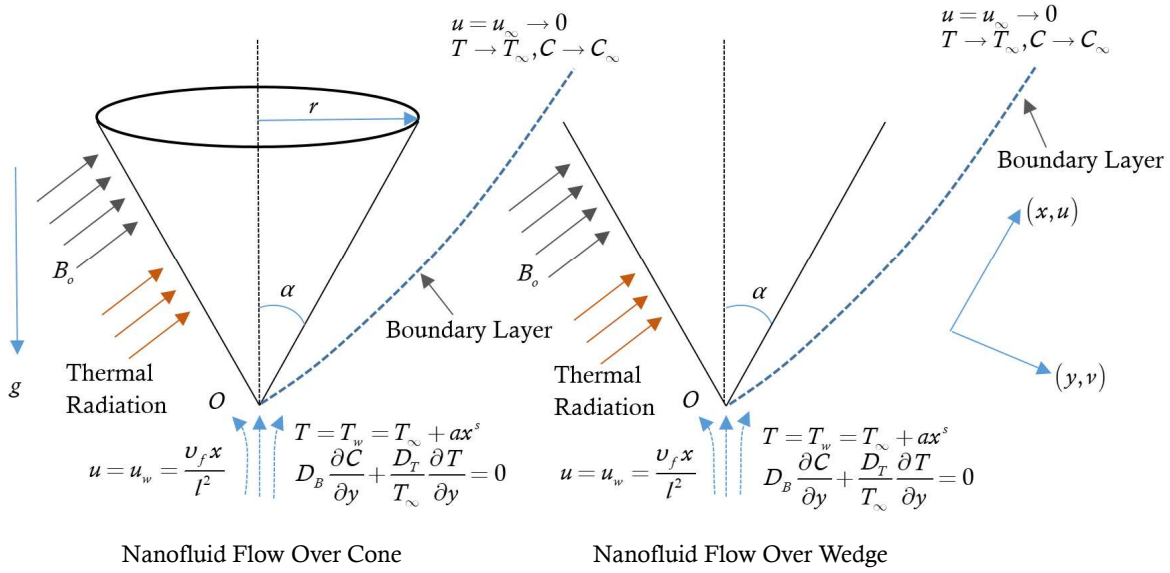

Fig. 1. Physical model of cone and wedge with coordinate system

The aspects of Brownian motion and thermophoresis together with thermal radiation and chemical reaction are taken into consideration. Cattaneo-Christov heat and mass flux models are applied to evaluate heat transfer, thermal and concentration diffusion instead of traditional Fourier's and Fick's models. Zero normal wall mass flux condition is retained to passively control the concentration of nanoparticle at the surface. The nanoparticles are spherical in shape. Based on above assumptions, the equation governing the boundary layer flow are reduced to the following form [54, 55]:

Continuity-equation

$$\frac{\partial\left(r^n u\right)}{\partial x} + \frac{\partial\left(r^n v\right)}{\partial y} = 0, \tag{1}$$

The thermal boundary layer is assumed to be thin and, therefore, r can be approximated by the local cone radius and written as $r = x\sin(\alpha)$.

Momentum-equation

$$\left(u\frac{\partial u}{\partial x} + v\frac{\partial u}{\partial y}\right) = \frac{\mu_{nf}}{\rho_{nf}}\left(\frac{\partial^2 u}{\partial y^2}\right) + \left[\left(1-C_\infty\right)\rho_{f\infty}\beta_{nf}\left(T-T_\infty\right)\right]\frac{g}{\rho_{nf}}\left(\cos\alpha\right) - \left[\left(\rho_p - \rho_{f\infty}\right)\left(C-C_\infty\right)\right]\frac{g}{\rho_{nf}}\left(\cos\alpha\right) - \frac{\sigma_{nf}}{\rho_{nf}}B_o^2 u \tag{2}$$

Above equations are subjected to following boundary conditions:

$$\left.\begin{aligned} &u = u_w = \frac{\upsilon_f x}{l^2},\ v = 0 \quad \text{at} \quad y = 0 \\ &u \to 0 \qquad \text{when } y \to \infty \end{aligned}\right\} \tag{3}$$

The present model corresponds to flow over two different geometries on account of following conditions [55, 56]:

(a) $n=0$ and $\alpha \neq 0$, represents flow over wedge.

(b) $n=1$ and $\alpha \neq 0$, represents flow over cone.

where, u and v represent velocity components in x and y directions respectively, g is acceleration by gravity, β is volumetric thermal expansion coefficient, υ is kinematic viscosity, σ is electrical conductivity, ρ is density, μ is dynamic viscosity and l is characteristic length.

With the use of following transformations (see [55, 56]) and parameters (refer to Table 1),

$$\left.\begin{aligned} &\eta=\frac{y}{l},\ u=\frac{\upsilon_f x}{l^2}f'(\eta),\quad v=-\upsilon_f\frac{(n+1)}{l}f(\eta),\ \mu_{nf}=\frac{\mu_f}{(1-\phi)^{2.5}},\frac{(\rho\beta)_{nf}}{(\rho\beta)_f}=(1-\phi)+\phi\frac{(\rho\beta)_p}{(\rho\beta)_f}=C_o,\\ &\frac{\rho_{nf}}{\rho_f}=(1-\phi)+\phi\frac{(\rho)_p}{(\rho)_f}=D,\frac{\sigma_{nf}}{\sigma_f}=\left[1+\frac{3(\sigma-1)\phi}{(\sigma+2)-(\sigma-1)\phi}\right]=F,\sigma=\frac{\sigma_p}{\sigma_f}\end{aligned}\right\} \tag{4}$$

The equation of continuity is identically satisfied and Eqns. (2) & (3) yield:

$$A f'''+D\left[(n+1)f f''-\left(f'\right)^2\right]-FM f'+\left(\frac{C_o}{D}\right)\lambda\,\Theta\cos\alpha-\lambda Nr\,\varphi\cos\alpha=0, \tag{5}$$

$$\left.\begin{aligned} &f=0,\ f'=1\ \text{ at }\eta=0\\ &f'\to 0\qquad \text{as }\ \eta\to\infty\end{aligned}\right\} \tag{6}$$

where $\lambda(=l^4 g\beta_f(1-C_\infty)(T_w-T_\infty)\rho_\infty/\rho_f v_f^2 x\equiv Gr_x/Re_x^2)$ is mixed convection parameter (sometimes referred as Richardson number), which is also ratio of local Grashof number $Gr_x(=g\beta_f(1-C_\infty)x^3\rho_{f_\infty}(T_w-T_\infty)/\upsilon_f^2\rho_f)$ to the local Reynolds number $Re_x(=u_w x/\upsilon_f)$. Physically, the negative values and positive of λ relates to cooling of nanofluid (or warming of surface) and heating of nanofluid (or cooling of surface), respectively. The other non-dimensional parameters are as such:

$M(=\sigma_f B_0^2 l^2/\rho_f\upsilon_f)$ is magnetic parameter, $Nr(=(\rho_p-\rho_{f_\infty})C_\infty/\beta_f(1-C_\infty)(T_w-T_\infty)\rho_{f_\infty})$ is buoyancy ratio parameter and $A(=(1-\varphi)^{-2.5})$ is the dimensionless parameter and prime denotes differentiation w.r.t η.

2.2 Heat and Mass transfer analysis by means of Cattaneo-Christov double diffusion theory

The Cattaneo-Christov double diffusion theory has been introduced in characterizing thermal and concentration diffusion with heat and mass fluxes relaxations, respectively. The expressions for heat flux $\boldsymbol{q}$ and mass flux $\boldsymbol{j}$ in terms of Cattaneo-Christov theory are as follows [44-49]:

$$\boldsymbol{q}+\tau_t\left[\frac{\partial\boldsymbol{q}}{\partial t}+\mathbf{v}.\nabla\boldsymbol{q}-\boldsymbol{q}.\nabla\mathbf{v}+(\nabla.\mathbf{v})\boldsymbol{q}\right]=-k\nabla T, \tag{7}$$

$$\boldsymbol{j}+\tau_c\left[\frac{\partial\boldsymbol{j}}{\partial t}+\mathbf{v}.\nabla\boldsymbol{j}-\boldsymbol{j}.\nabla\mathbf{v}+(\nabla.\mathbf{v})\boldsymbol{j}\right]=-D_B\nabla C, \tag{8}$$

where τ_t and τ_c denotes heat flux relaxation time and mass flux relaxation time, respectively. The symbol k stands for thermal conductivity, D_B for Brownian diffusivity and $\mathbf{v}$ denotes velocity. The classical Fourier's and Fick's law can be obtained by substituting $\tau_t=\tau_c=0$ in Eqns. (7) and (8). Now, utilizing the steady state conditions ($\partial\boldsymbol{q}/\partial t=0$ and $\partial\boldsymbol{j}/\partial t=0$) and mass continuity equation $(\nabla.\mathbf{v}=0)$, eqns. (7) and (8) reduce to following form,

$$\boldsymbol{q}+\tau_t\left[\mathbf{v}.\nabla\boldsymbol{q}-\boldsymbol{q}.\nabla\mathbf{v}\right]=-k\nabla T, \tag{9}$$

$$\boldsymbol{j}+\tau_c\left[\mathbf{v}.\nabla\boldsymbol{j}-\boldsymbol{j}.\nabla\mathbf{v}\right]=-D_B\nabla C, \tag{10}$$

Table 1. Thermo-physical properties of water and Copper (*Cu*) nanoparticles [56].

	ρ (Kg/m^3)	C_p (J/KgK)	k (W/mK)	β (1/K)	σ (S/m)
Water	997.1	4179	0.613	21.4×10^{-6}	0.005
Copper (Cu)	8933	385	401	17×10^{-6}	5.98×10^{7}

The two-dimensional energy and concentration equations for the present case attain the following forms:

$$\left(\rho C_p\right)_{nf}\left(u\frac{\partial T}{\partial x}+v\frac{\partial T}{\partial y}\right)+\left(\rho C_p\right)_{nf}\tau_t\zeta_t=k_{nf}\frac{\partial^2 T}{\partial y^2}+\tau\left(\rho C_p\right)_{nf}\left[D_B\frac{\partial T}{\partial y}\frac{\partial C}{\partial y}+\frac{D_T}{T_\infty}\left(\frac{\partial T}{\partial y}\right)^2\right]-\frac{\partial q_r}{\partial y} \tag{11}$$

$$\left(u\frac{\partial C}{\partial x}+v\frac{\partial C}{\partial y}\right)+\tau_c\zeta_c=D_B\frac{\partial^2 C}{\partial y^2}+\frac{D_T}{T_\infty}\left(\frac{\partial^2 T}{\partial y^2}\right)-K_o\left(C-C_\infty\right) \tag{12}$$

In the above equations (11) and (12), the Cattaneo-Christov expressions are as follows:

$$\zeta_t=u^2\frac{\partial^2 T}{\partial x^2}+\left(u\frac{\partial u}{\partial x}+v\frac{\partial u}{\partial y}\right)\frac{\partial T}{\partial x}+\left(u\frac{\partial v}{\partial x}+v\frac{\partial v}{\partial y}\right)\frac{\partial T}{\partial y}+2uv\frac{\partial^2 T}{\partial x\partial y}+v^2\frac{\partial^2 T}{\partial y^2} \tag{13}$$

$$\zeta_c=u^2\frac{\partial^2 C}{\partial x^2}+\left(u\frac{\partial u}{\partial x}+v\frac{\partial u}{\partial y}\right)\frac{\partial C}{\partial x}+\left(u\frac{\partial v}{\partial x}+v\frac{\partial v}{\partial y}\right)\frac{\partial C}{\partial y}+2uv\frac{\partial^2 C}{\partial x\partial y}+v^2\frac{\partial^2 C}{\partial y^2} \tag{14}$$

The associated boundary conditions with eqns. (11) and (12) are:

$$\left.\begin{aligned}&T=T_w=T_\infty+ax^s,\ D_B\frac{\partial C}{\partial y}+\frac{D_T}{T_\infty}\frac{\partial T}{\partial y}=0\ \text{ at }\ \mathrm{y}=0\\&T\to T_\infty,\ C\to C_\infty\quad\ \text{when }\ \mathrm{y}\to\infty\end{aligned}\right\} \tag{15}$$

where C_p stands for specific heat, τ for ratio of effective heat capacity of the solid nanoparticle to the base fluid, $q_r=-(4\sigma^*/3k_{nf}^*)(\partial T^4/\partial y)$ stands for radiation heat flux, σ^* is Stefan-Boltzmann constant, k_{nf}^* is the mean absorption coefficient, D_T thermophoretic diffusion coefficient and K_o is reaction rate. Assuming the sufficiently low temperature difference in the flow, the following relationship holds:

$$T^4\cong 4T_\infty^3T-3T_\infty^4 \tag{16}$$

Using the following transformation (see [55, 56]) and nanofluid parameters (see Table 1),

$$\left.\begin{aligned}&\Theta(\eta)=\frac{T-T_\infty}{T_w-T_\infty},\ \varphi(\eta)=\frac{C-C_\infty}{C_\infty},\\&\frac{\left(\rho C_p\right)_{nf}}{\left(\rho C_p\right)_f}=(1-\phi)+\phi\frac{\left(\rho C_p\right)_p}{\left(\rho C_p\right)_f}=B,\ \frac{k_{nf}}{k_f}=\frac{\left(k_p+2k_f\right)-2\phi\left(k_f-k_p\right)}{\left(k_p+2k_f\right)+\phi\left(k_f-k_p\right)}=E\end{aligned}\right\} \tag{17}$$

along with eqns. (4) and (16), eqns. (11), (12) and (15) become

$$\left.\begin{aligned}&\frac{E}{B\,Pr}\left[1+\frac{4}{3}Rd\right]\Theta''+Nb\,\Theta'\varphi'+Nt\,\Theta'^2-s\,f'\Theta+(n+1)f\Theta'\\&-\gamma_t\left[\begin{aligned}&s(s-1)f'^2\Theta+(n+1)^2f^2\Theta''+(n+1)^2ff'\Theta'\\&+sf'^2\Theta-(n+1)sff''\Theta-2(n+1)sff'\Theta'\end{aligned}\right]=0\end{aligned}\right\}, \tag{18}$$

$$\varphi''+(n+1)Sc\,f\varphi'+\left(\frac{Nt}{Nb}\right)\Theta''-Sc\,Kr\,\varphi-\gamma_c\,Sc(n+1)^2\left[f^2\varphi''+ff'\varphi'\right]=0, \tag{19}$$

$$\left.\begin{aligned}&\Theta=1,\ \varphi'+\left(\frac{Nt}{Nb}\right)\Theta'=0\ \text{ at }\ \eta=0\\&\Theta\to 0,\ \ \varphi\to 0\quad\ \text{as }\ \eta\to\infty\end{aligned}\right\} \tag{20}$$

where $Pr(=(\rho C_p)_f\upsilon_f/k_f)$ stands for Prandtl number, $Rd(=4\sigma^*T_\infty^3/k_{nf}^*k_{nf})$ is thermal radiation parameter, $Nb(=D_BC_\infty\tau/\upsilon_f)$ is Brownian motion parameter, $Nt(=\tau D_Tax^s/T_\infty\upsilon_f)$ is thermophoresis parameter, $\gamma_t(=\tau_t\upsilon_f/l^2)$ is the thermal relaxation time parameter, $\gamma_c(=\tau_c\upsilon_f/l^2)$ is the solutal relaxation time parameter, $Kr(=K_o\,l^2/\upsilon_f)$ is the chemical reaction rate parameter and $Sc(=\upsilon_f/D_B)$ is the Schmidt number.

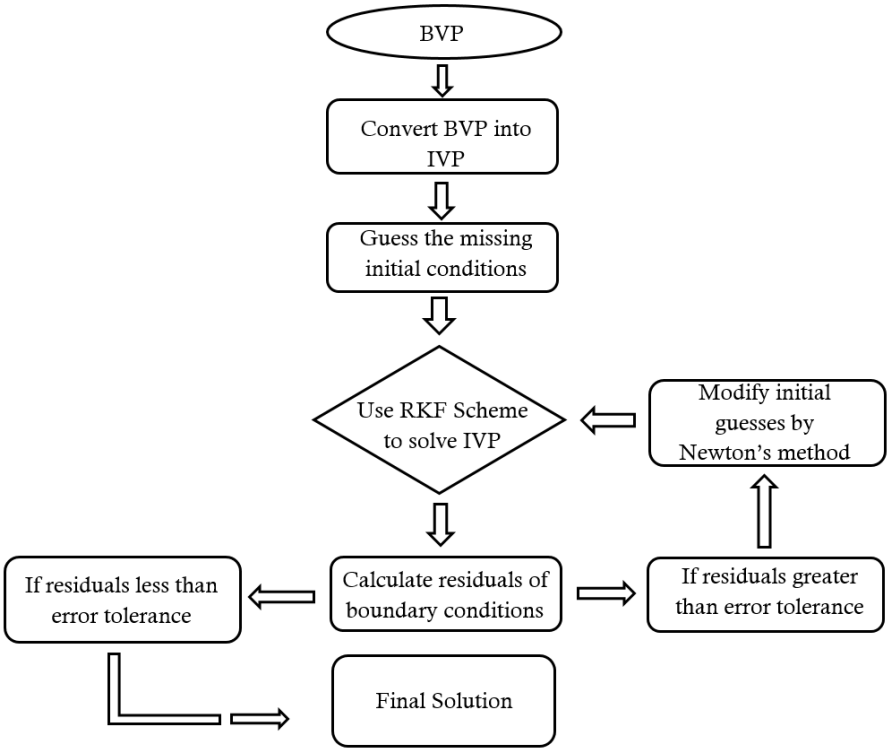

Fig. 2. Flow chart of shooting method

2.3 Quantities related to engineering interest

Skin friction coefficient

$$C_f^* = C_f \sqrt{Re_x} = \frac{f''(0)}{(1-\phi)^{2.5}} \tag{21}$$

and, wall heat transfer coefficient

$$Nu_x^* = \frac{Nu}{\sqrt{Re_x}} \frac{k_f}{k_{nf}} = -\left(1+\frac{4}{3}Rd\right)\Theta'(0) \tag{22}$$

The Sherwood number which helps in characterizing the dimensionless mass transfer rate at surface is identically zero because of zero normal wall mass flux condition (see eqn. 15). So, in this study we focus our attention only to skin friction coefficient and non-dimensional wall heat transfer coefficient.

3. Numerical Method

Runge-Kutta-Fehlberg method with shooting technique (refer to Fig. 2) are utilized to solve the dimensionless eqns. (5), (18) and (19), which represents the modeled problem together with boundary conditions (6) & (20). We substitute $g_1 = f$, $g_2 = f'$, $g_3 = f''$, $g_4 = \Theta$, $g_5 = \Theta'$, $g_6 = \varphi$, $g_7 = \varphi'$ and seven first ODEs equations were formed as such:

$$\left.\begin{aligned}
&g_1' = g_2\ ;\ g_1(0) = 0\\
&g_2' = g_3\ ;\ g_2(0) = 1\\
&g_3' = \frac{1}{A}\left[-D\left((n+1)g_1g_3 - g_2^2\right) + M\,F\,g_2 - \left(\frac{C_o}{D}\right)\lambda\, g_4\cos(\alpha) + \lambda Nr\, g_6\cos(\alpha)\right];\ g_3(0) = h_1\\
&g_4' = g_5;\ g_4(0) = 1\\
&g_5' = \left\{\gamma_t\left[s(s-1)g_2g_2g_4 + (n+1)^2\, g_1g_2g_5 + sg_2g_2g_4 - (n+1)sg_1g_3g_4 - 2(n+1)sg_1g_2g_5\right] - Nb\, g_5\, g_7 - Nt\, g_5\, g_5\right.\\
&\left. + s\, g_2\, g_4 - (n+1)g_1\, g_5\right\} \times \left\{\left(\frac{E}{B\,Pr}\right)\left(1+\frac{4}{3}Rd\right) - \gamma_t(n+1)^2\, g_1g_1\right\}^{-1};\ g_5(0) = h_2\\
&g_6' = g_7;\ g_6(0) = h_3\\
&g_7' = \left\{-(n+1)Sc\, g_1g_7 - (Nt/Nb)g_5' + Sc\,Kr\, g_6 + \gamma_c\, Sc(n+1)^2\, g_1g_2g_7\right\} \times \left\{1 - \gamma_c\, Sc(n+1)^2\, g_1g_1\right\}^{-1};\ g_7(0) = -\frac{Nt}{Nb}h_2
\end{aligned}\right\} \tag{23}$$

Table 2. Values of missing slopes found by shooting method with different value of $\eta_{\max}$.

	Cone			Wedge		
$\eta_{\max}$	$f''(0)$	$\Theta'(0)$	$\phi(0)$	$f''(0)$	$\Theta'(0)$	$\phi(0)$
1	-1.4785021	-2.931907	-0.88010	-1.363458	-2.472050	-0.9242810
2	-1.2699781	-3.004657	-0.75879	-1.109958	-2.508200	-0.8208510
4	-1.2477481	-3.014407	-0.69310	-1.073790	-2.525550	-0.7393200
6	-1.2477481	-3.014507	-0.68354	-1.072995	-2.526215	-0.7216800
8	-1.2478511	-3.014530	-0.68215	-1.073164	-2.526215	-0.7179050
10	-1.2478751	-3.014530	-0.68196	-1.073225	-2.526195	-0.7170900

Table 3. Comparison of values of $f''(0)$ & $-\theta'(0)$ with results of Vajravelu and Nayfeh [55] for the flow over cone.

					Present results		Vajravelu and Nayfeh [55]	
Q	Pr	Gr	M	s	$f''(0)$	$-\theta'(0)$	$f''(0)$	$-\theta'(0)$
-5	0.3	-0.5	1	-2.1	-0.15559221	-2.2374764635	-0.155592	-2.237475
-5	0.3	-0.5	1	2.1	-0.15600196	-2.23278567	-0.156001	-2.232780
-5	0.3	-0.5	3	2.1	-0.12640183	-2.23373586	-0.126400	-2.233732
1	1.0	0.5	3	2.1	0.32899477	0.79855920	0.328994	0.798537

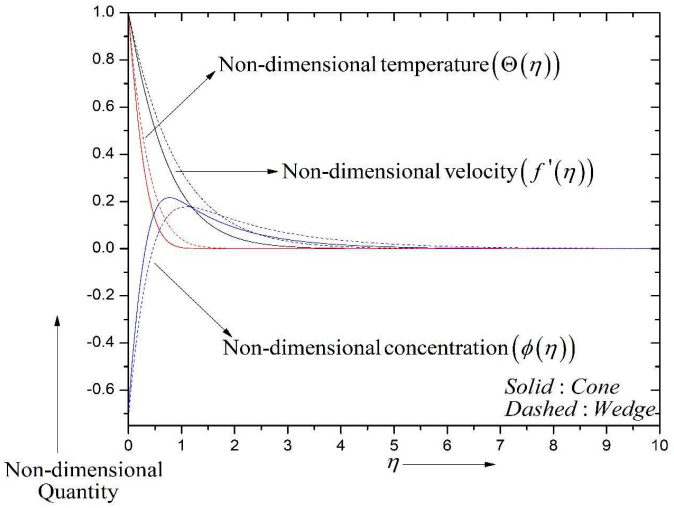

Fig. 3. A representative case to present the behavior of non-dimensional velocity, temperature and concentration as nanofluid moves towards ambient field.

Process of finding the solution of system of equations (23) is initialized by finding the missing slopes i.e., $h_1 = f''(0)$, $h_2 = \Theta'(0)$ and $h_3 = \varphi'(0)$ (see Table 2). The numerical computations are stopped when following conditions is met, $\max\{|g_2(\eta_{\max})-0|, |g_4(\eta_{\max})-0|, |g_6(\eta_{\max})-0|\} \le 10^{-5}$ (error tolerance). All the calculations and results are obtained for $\eta_{\max} = 10$. All the ambient boundary conditions are attained asymptotically (see Fig. 3). For the validation of our results, we present a comparison with Vajravelu and Nayfeh [55] results under the special case in Table [3].

4. Results and Discussion

This segement focus on physical justifications of the effects of related parameters on specific flow properties. For numerical computations, the default values were set as:
$\phi = 0.01$, $M = 0.2$, $\lambda = 0.4$, $Nr = 0.2$, $Pr = 6.2$, $Rd = 0.2$, $\gamma_t = 0.05$, $\gamma_c = 0.05$, $s = 1$, $\alpha = \pi/3$, $Nb = 0.2$, $Nt = 0.2$, $Sc = 0.5$ and $Kr = 0.2$. The variation, if any, of the values from set default is pointed out in the table or figure.
Tables 4, 5 and 6 are outlined to present the numerical values of skin friction and heat transfer coefficient in case of cone and wedge. Skin friction coefficient is seen to increase with increase in the value of magnetic parameter M but it decreases with mixed convection parameter λ. It implies that resisting force on the surface of cone or wedge increases with increasing strength of magnetic parameter and decreases as mixed convection parameter is increased. The increase in volume fraction ϕ also results in increment in surface drag. The skin friction coefficient for the aforementioned cases was found to be higher in case of flow over the cone in comparison to wedge case. The change in value of skin friction coefficient for rest of the parameters was not found to be significant. The numerical values of wall heat transfer rate elucidates that with increment in strength of thermal radiation parameter Rd, thermal relaxation parameter γ_t and wall temperature related parameter s, the heat transfer rate also amplifies. For the other case, a marginal reduction in heat transfer rate was seen as the value of parameter M and ϕ is incremented. Thermophoresis parameter Nt is the ratio of

thermophoretic diffusion caused by temperature difference to the momentum diffusion in the nanofluid. An increase in the value of *Nt*, causes nanoparticles near the heated surface to move towards the ambient fluid. This leads to increase in nanofluid thermal diffusivity and increase in thermal boundary layer thickness. Now, with the increase in width of thermal boundary layer, heat transfer rate through surface of cone or wedge decreases. The heat transfer rate was found to be lower in case of flow over the wedge in comparison to flow over the cone for all above discussed cases. The change in value of heat transfer rate for rest of the parameters was not found to be significant. The Brownian motion parameter *Nb* also does not change the heat transfer rate significantly despite being present in the energy equation. The reason for the case can be explained with the use of boundary conditions (20) in energy equation (18) (as $\eta \to 0$), as resulting equation for energy becomes independent of term *Nb*.

Table 4. Numerical values of skin friction & heat transfer coefficients of Cu-water nanofluid for variation in *M, Nr,* λ and ϕ.

M	Nr	λ	ϕ	$-C_f^*$		Nu_x^*	
				Cone	Wedge	Cone	Wedge
0.2				1.27963	1.10053	3.818405	3.199847
0.4				1.35564	1.18875	3.793920	3.170581
0.8				1.49729	1.34871	3.748257	3.117197
1.2				1.62763	1.49233	3.706077	3.068943
	0.2			1.27963	1.10053	3.818405	3.199847
	0.5			1.28159	1.09973	3.815770	3.197770
	1			1.28555	1.09904	3.811147	3.193970
		-2		1.49766	1.39384	3.777947	3.137473
		0		1.31539	1.14820	3.811907	3.190100
		1		1.22640	1.02985	3.827930	3.214040
		2		1.13875	0.91416	3.843282	3.236663
			0.01	1.27963	1.10053	3.818405	3.199847
			0.02	1.34145	1.15351	3.742493	3.136748
			0.03	1.40338	1.20660	3.669027	3.075593

Table 5. Numerical values of skin friction & heat transfer coefficients of Cu-water nanofluid for variation in *Rd,* γ_t , *s* and *Nt*.

Rd	γ_t	s	Nt	$-C_f^*$		Nu_x^*	
				Cone	Wedge	Cone	Wedge
0.2				1.27963	1.10053	3.818405	3.199847
0.5				1.27478	1.09437	4.305333	3.609867
0.8				1.27049	1.08900	4.720308	3.960291
	0.0			1.27752	1.09889	3.653662	3.094796
	0.05			1.27963	1.10053	3.818405	3.199847
	0.1			1.28150	1.10207	3.982210	3.303511
		1.0		1.27963	1.10053	3.818405	3.199847
		1.5		1.28164	1.10441	4.301499	3.753893
		2.0		1.28339	1.10756	4.761261	4.266095
			0.2	1.27963	1.10053	3.818405	3.199847
			0.5	1.28103	1.09904	3.762507	3.163342
			0.8	1.28280	1.09779	3.706077	3.126627

Table 6. Numerical values of skin friction & heat transfer coefficients of Cu-water nanofluid for variation in *Nb,* γ_c , *Sc* and *Kr*.

Nb	γ_c	Sc	Kr	$-C_f^*$		Nu_x^*	
				Cone	Wedge	Cone	Wedge
0.2				1.27963	1.10053	3.818405	3.199847
0.5				1.27890	1.10093	3.819355	3.200651
0.8				1.27873	1.10103	3.819633	3.200848
	0			1.27929	1.10037	3.817860	3.199714
	0.05			1.27963	1.10053	3.818405	3.199847
	0.1			1.27993	1.10070	3.818911	3.199986
	0.5			1.28184	1.10195	3.822648	3.200974
	1.0			1.28258	1.10335	3.825587	3.202203
		0.5		1.27963	1.10053	3.818405	3.199847
		1.0		1.27868	1.10032	3.787447	3.180385
		2.0		1.27773	1.09979	3.733057	3.146907
			0.2	1.27963	1.10053	3.818405	3.199847
			0.5	1.27842	1.09927	3.811843	3.191582
			1.0	1.27753	1.09858	3.800190	3.177902

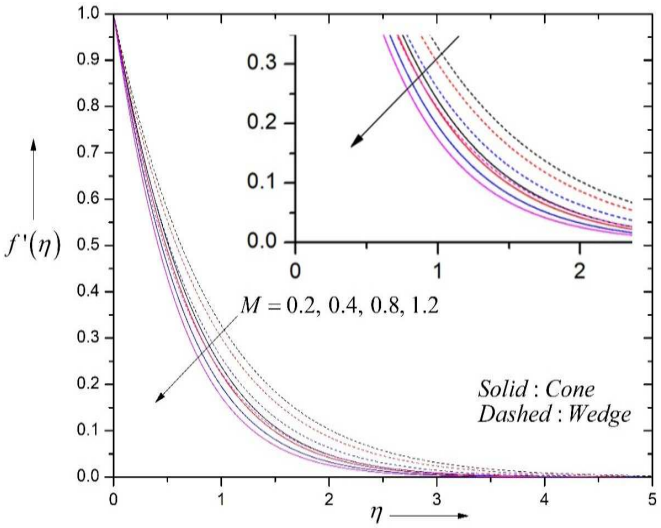

Fig. 4. Behavior of non-dimensional velocity with variation in magnetic field.

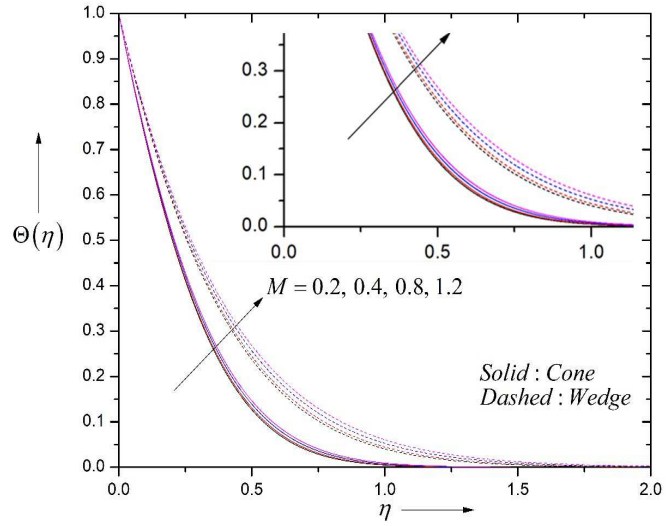

Fig. 5. Behavior of non-dimensional temperature with variation in magnetic field.

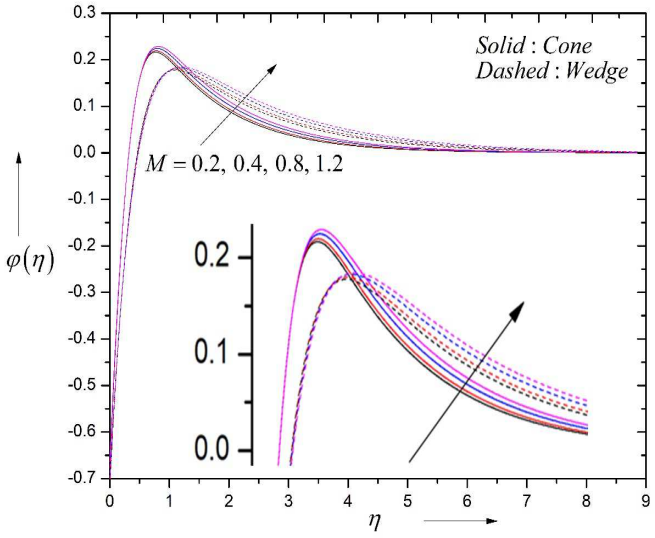

Fig. 6. Behavior of non-dimensional concentration with variation in magnetic field.

Velocity profiles, represented by f', are plotted at various values of magnetic parameter M in Fig. 4. A decreasing trend in f' is witnessed as M varies from $M = 0.2$ to $M = 1.2$. It means that the flow is retarded by the increasing magnetic parameter and this result agrees with the expectations. As, the increase in value of M, also leads to increase the Lorentz

force and it opposes the flow. Consequently, the decreasing trend in velocity is witnessed. Also, the momentum boundary layer thickness decreases with M. From Fig. 4, it can be observed that velocity is higher for the flow over wedge than flow over cone for all considered values of magnetic parameter. In Fig. 5, the graph of Θ for varying values of M are presented at mentioned default values of other parameters. As mentioned in the above discussion, decreasing velocity and increasing surface drag with increase in magnetic parameter causes the release of more amount of heat in the nanofluid flow, which increases the temperature and thermal boundary layer thickness of nanofluid flow. The temperature profiles are found to be significantly higher for the nanofluid flow over a wedge than for the case of nanofluid flow over a cone.

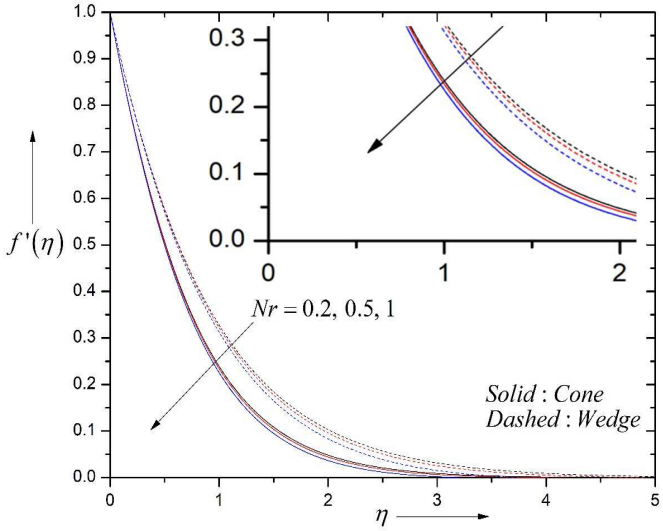

Fig. 7. Behavior of non-dimensional velocity with variation in buoyancy ratio parameter.

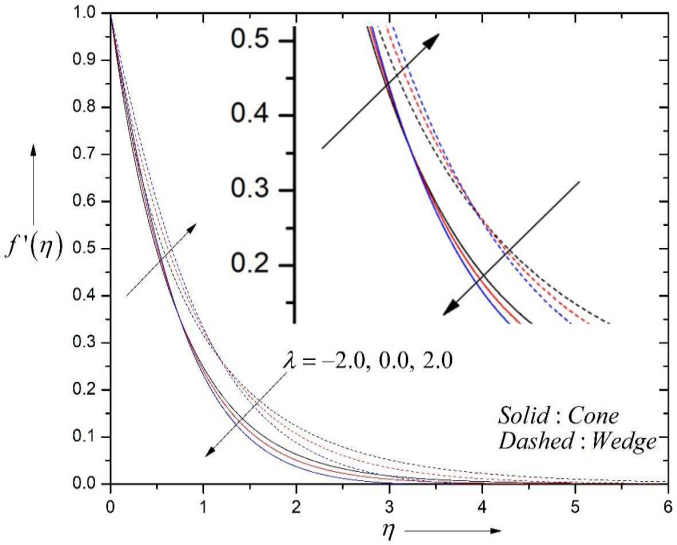

Fig. 8. Behavior of non-dimensional velocity with variation in mixed convection parameter.

The behavior of nanoparticles concentration profile for the change in value of M is recorded in Fig. 6. The non-dimensional nanoparticle concentration φ is seen to be negative at the surface of cone or wedge. Physically this situation means, the effect of thermophoresis is such that elevated wall temperature above the ambient conditions corresponds to depression in nanoparticle concentration at the surface of cone or wedge below the ambient condition. An overshoot in concentration profiles is witnessed which illustrates that concentration profiles in vicinity of plate exceeds the free stream nanoparticle concentration. It is obvious from the transformation and boundary conditions that φ would be negative at the surface of cone or wedge (at $\eta = 0$). It is also seen that, such an outcome persists for any value of other pertinent parameters. Literature search revealed that, this present outcome for the variation in nanoparticle concentration as fluid moves from surface to the far field is consistent with the previously published work (see [7] and [32]) in which same boundary condition as present study for φ is considered. It is observed that after reaching an absolute maximum, the nanoparticle concentration is higher for higher value of M and nanoparticle concentration was found to be higher for flow over wedge. However, the value of absolute maximum for nanoparticle concentration was found to be higher in case of flow over cone.

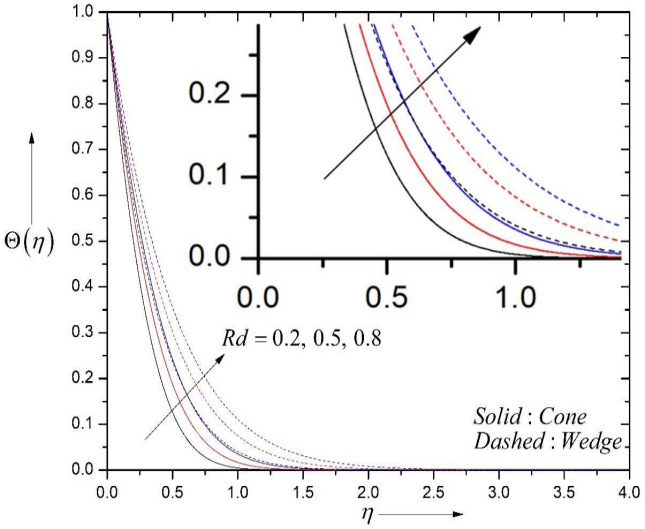

Fig. 9. Behavior of non-dimensional temperature with variation in thermal radiation parameter.

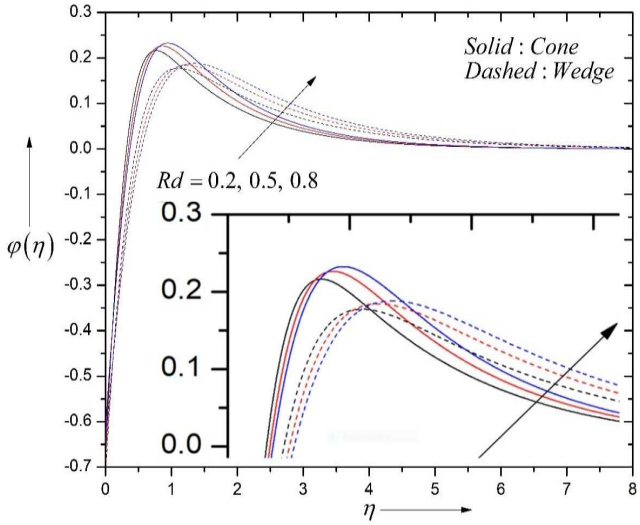

Fig. 10. Behavior of non-dimensional concentration with variation in thermal radiation parameter.

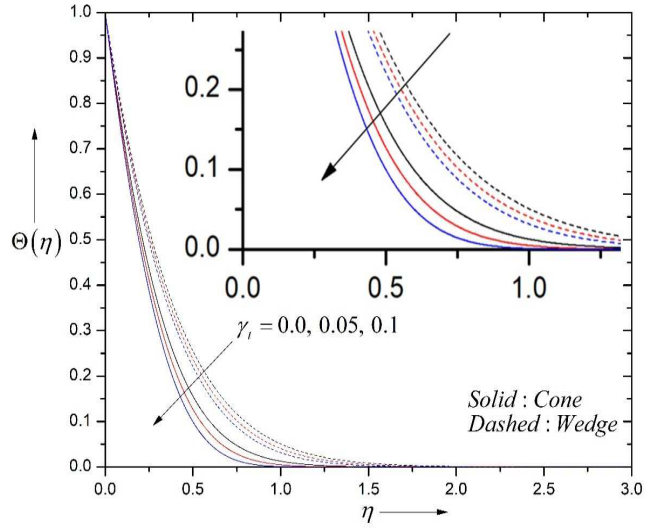

Fig. 11. Behavior of non-dimensional temperature with variation in thermal relaxation parameter

Figure 7 deals with variation in velocity for different values of buoyancy ratio parameter *Nr*. For an increase in the value of *Nr*, the velocity was seen to decrease. The velocity for flow over wedge was found higher in comparison to flow over cone when changing the values of *Nr*.

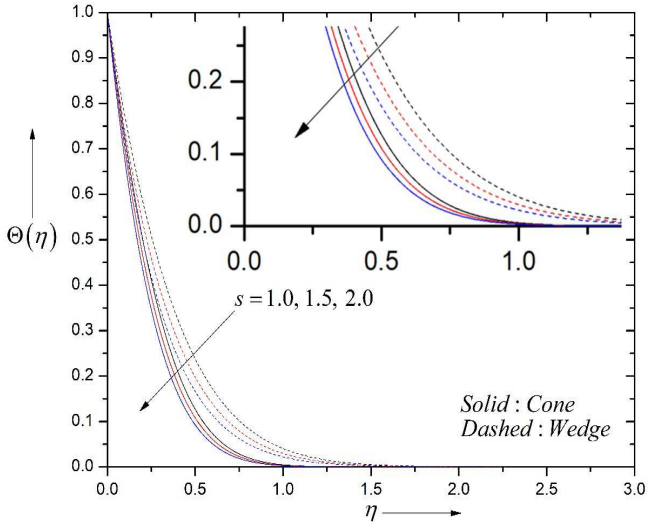

Fig. 12. Behavior of non-dimensional temperature with variation in wall temperature related parameter.

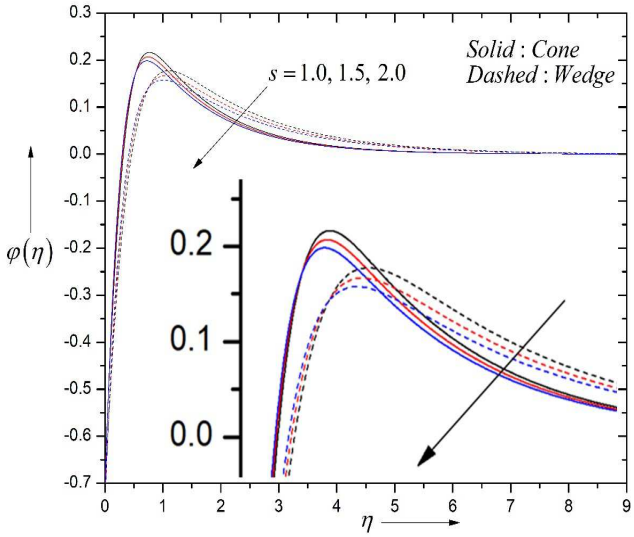

Fig. 13. Behavior of non-dimensional concentration with variation in wall temperature related parameter.

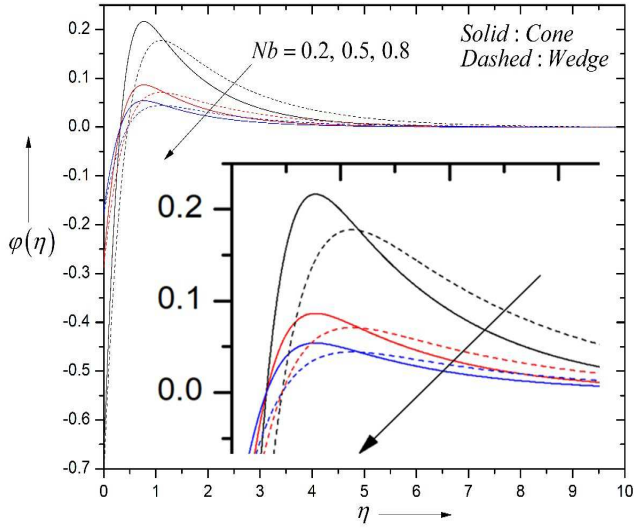

Fig. 14. Behavior of non-dimensional concentration with variation in Brownian motion parameter.

Figure 8 presents the curves of f' for various values of λ, when other parameters are fixed. Initially, increasing the value of λ, leads to increase in velocity but after a certain distance opposite trend is observed. The distance where this change in trend is observed is found more near to surface in case of flow over cone. However, velocity was found higher in case

of flow over wedge on changing λ and keeping other parameters fixed. In Figs. 9 and 10, temperature and concentration profiles are plotted at different numerical values of *Rd*. As expected, temperature was to seen to rise with increasing value of thermal radiation parameter *Rd*. The mean absorption coefficient decreases as thermal radiation increases, which leads to increase in radiative heat transfer and consequently, the temperature rises. Substantial rise in temperature with change in numerical values of parameter *Rd* was seen and temperature was found higher in case of flow over wedge. From Fig. 10, it is concluded that after attaining the absolute maximum, when nanofluid moves towards far field, concentration of nanoparticles rises as parameter *Rd* increases. The value of absolute maximum for concentration of nanoparticles was higher for flow over cone but the concentration was found higher for flow over wedge as fluid moved towards the far field.

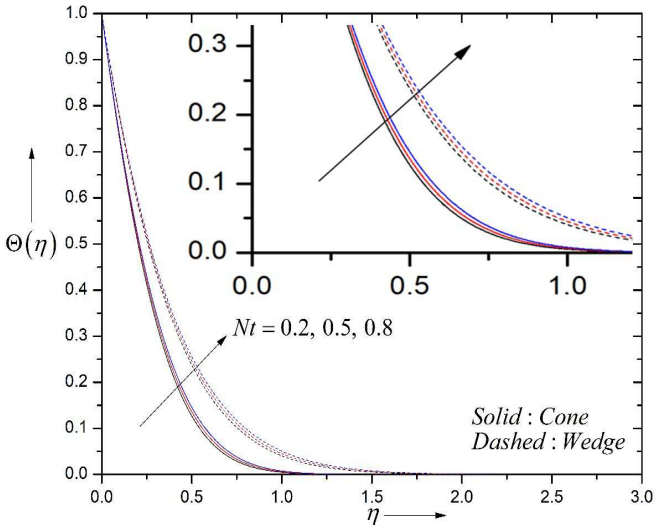

Fig. 15. Behavior of non-dimensional temperature with variation in thermophoresis parameter.

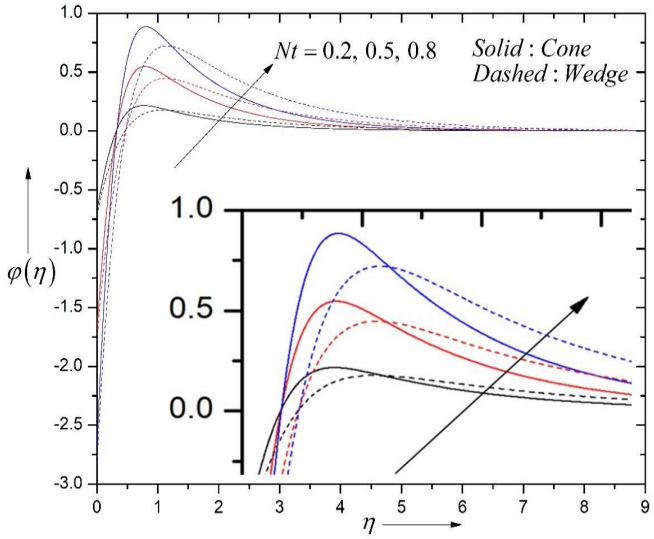

Fig. 16. Behavior of non-dimensional concentration with variation in thermophoresis parameter.

Figure 11 points out the change in temperature distribution Θ as the thermal relaxation parameter γ_t increases. Temperature is seen to have an inverse relationship with thermal relaxation parameter. It substantiates the Cattaneo-Christov theory that higher values of γ_t, physically means that they require more amount of time to transfer heat to particles with low energy when a temperature gradient is present in medium. It is to be noted that for $\gamma_t = 0$, it represents Fourier's law of heat conduction and for this situation heat transfers without any time lag through the whole medium. From Fig. 11, it can be observed that temperature is dominant for the case $\gamma_t = 0$ (Fourier's model) than $\gamma_t \neq 0$ (C-C model). It can be said that C-C model helps characterize the conducting or non-conducting nature of a material. As, higher the value of thermal relaxation parameter of a material or higher the time a material takes to transfer heat, the more non-conducting it is in nature.

The changes in temperature and concentration profiles due to varying values of wall temperature related parameter *s* are presented in Figs. 12 and 13, respectively. Both temperature and nanoparticle concentration decrease as the value of

parameter s enlarges from $s=1$ to $s=2$. Temperature profile for flow over cone is lower than flow over wedge. It is to be noted that $s=0$ represents the isothermal boundary condition at wall ($\eta=0$). From Fig. 13, it is evident that wall temperature of the cone or wedge also regulates the nanoparticle concentration as fluid moves towards far field. Concentration for flow over wedge was found higher when fluid moved away from wall. Fig. 14 presents the relationship between parameter *Nb* and concentration φ when other parameters are kept constant. We observed that with higher value of *Nb*, the value of absolute maximum of nanoparticle concentration decreases. Also, a significant decay in concentration was seen when value of *Nb* is varied from $Nb=0.2$ to $Nb=0.8$. Negligible variation in temperature profiles was noticed with change in parameter *Nb*, due to boundary condition $\varphi'(0)=-(Nt/Nb)\Theta'(0)$ in eqn. (18) when we move towards wall. The result is in accordance with Kuznetsov and Nield [50, 51] who were first to study the zero wall mass flux condition.

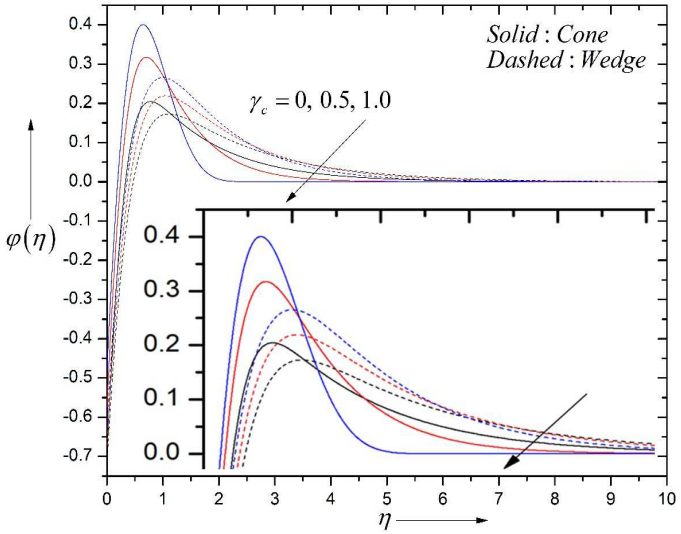

Fig. 17. Behavior of non-dimensional concentration with variation in solutal relaxation parameter.

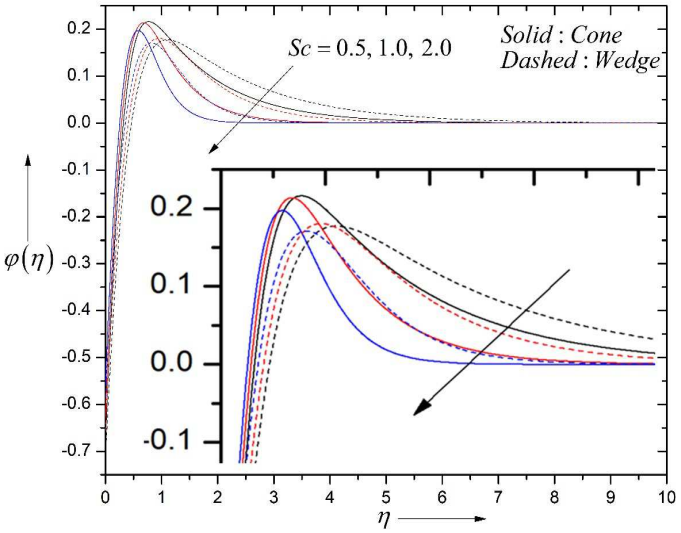

Fig. 18. Behavior of non-dimensional concentration with variation in Schmidt number.

Influence of thermophoresis parameter *Nt* on temperature and concentration is elucidated in Figs. 15 and 16. Intensification in strength of thermophoretic force leads to deeper migration of solid nanoparticles to far field fluid. This leads to thickening of thermal boundary layer and enhancement in temperature of nanofluid.

Figure 16 tells that the value of absolute maximum of concentration increases rapidly with small increase in parameter *Nt*. After attaining the absolute maximum, the concentration was found higher for higher values of *Nt*. The flow over wedge has higher concentration of nanoparticles when fluid moves towards ambient field but lower value for absolute maximum in each case when *Nt* is varied. The variation in concentration profile for flow over wedge and cone under same physical conditions but for varying solutal relaxation time parameter γ_c is depicted in Fig. 17. On increasing the parameter γ_c, the concentration rises steeply to reach an absolute maximum and then to fall downwards. When fluid moves to far field, the concentration decreases with increasing value of parameter γ_c.

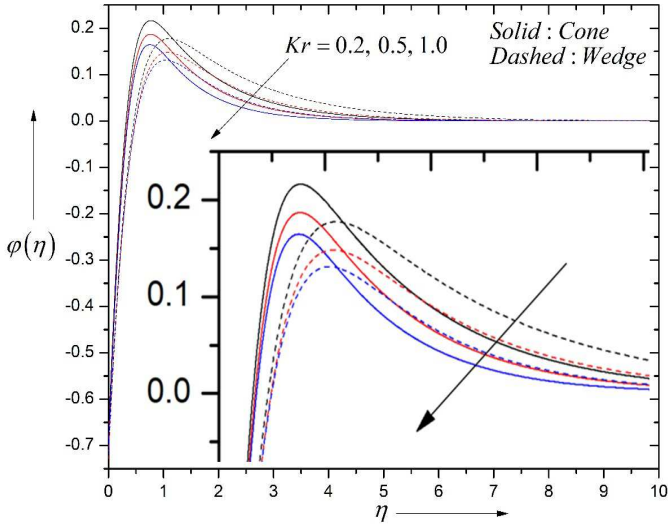

Fig. 19. Behavior of non-dimensional concentration with variation in chemical reaction parameter.

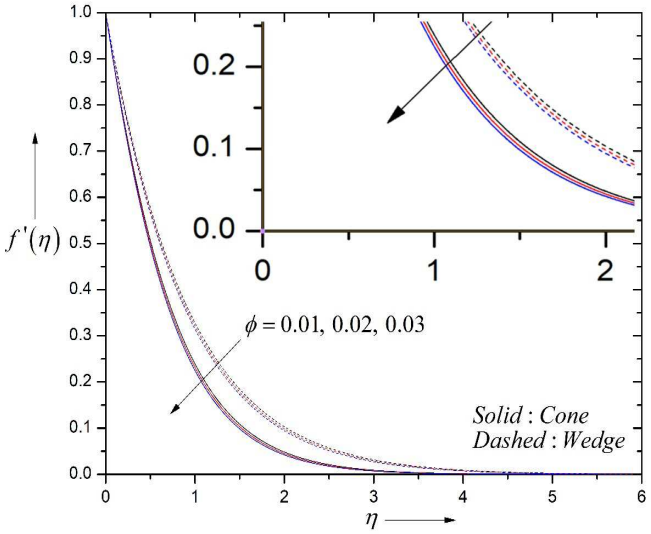

Fig. 20. Behavior of non-dimensional velocity with variation in volume fraction.

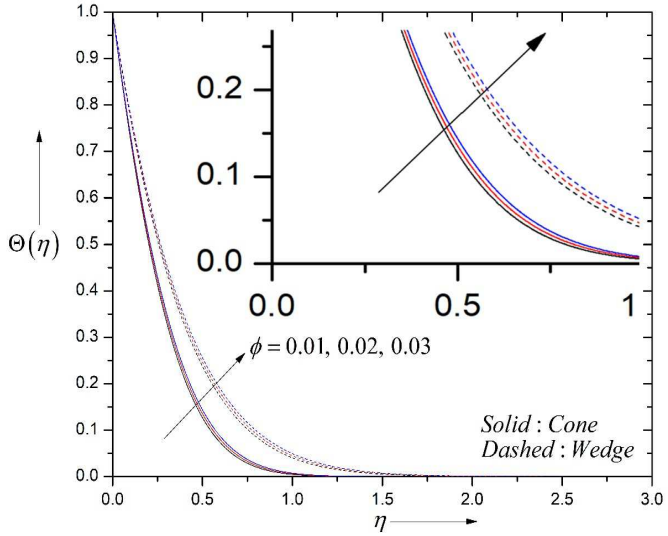

Fig. 21. Behavior of non-dimensional temperature with variation in volume fraction.

Fig. 18 portrays the impact of Schmidt number *Sc* on concentration profiles. Schmidt number is characterized as ratio of kinematic viscosity (υ_f) to the Brownian diffusion coefficient (D_B). The higher values of *Sc* relates to smaller values of D_B. Thus, increasing *Sc* means hampering the development of concentration boundary layer and consequently,

concentration reduces for higher values of *Sc*. The effect of chemical reaction parameter *Kr* on nanoparticle concentration is displayed via Fig. 19. After reaching the absolute maximum, when concentration starts to fall, the increasing value of *Kr* corresponds to decreasing concentration. The concentration profiles for flow over cone are lower than flow over wedge. The behavior of solution profiles of velocity, temperature and concentration with volume fraction ϕ is analyzed in Figs. 20, 21 and 22, respectively. The velocity was seen to decrease, whereas the temperature and concentration were found to increase with increasing volume fraction. The flow over wedge witnessed the higher velocity, temperature and concentration when nanofluid moves to far field on changing volume fraction.

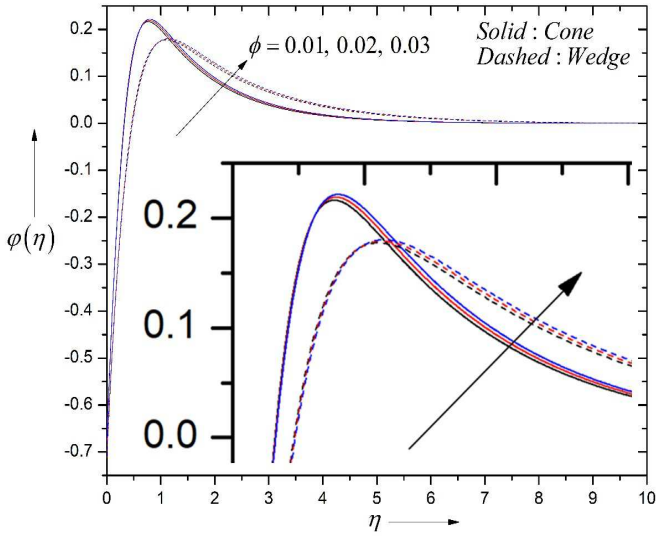

Fig. 22. Behavior of non-dimensional concentration with variation in volume fraction.

5. Conclusions

In this study, the authors have comparatively studied the flow over a vertical cone and wedge of Cu-water nanofluid using effective models of thermal conductivity and viscosity. The effects of mixed convection, thermal radiation and chemical reaction are discussed. Moreover, we have utilized the zero mass flux condition at the surface of cone and wedge. Furthermore, the modeled nanofluid problem is characterized by single phase nanofluid model (i.e., Tiwari and Das's model) and two phase mixture nanofluid model (i.e., Buongiorno's model) together with Cattaneo-Christov double diffusion model. The significant findings are summarized below:

1. For a particular set of values of parameters, the solution profiles of velocity, temperature and concentration were found higher in case of flow over wedge than flow over cone.
2. The temperature and concentration decrease with thermal relaxation parameter γ_t and solutal relaxation time parameter γ_c, respectively.
3. The velocity profiles experience the fall in their values when magnetic parameter *M*, buoyancy ratio parameter *Nr* and volume fraction ϕ increases.
4. The nanofluid temperature can be enhanced by increasing the magnetic parameter *M*, thermal radiation parameter *Rd*, thermophoresis parameter *Nt* and volume fraction ϕ.
5. The Brownian motion parameter *Nb* had no effect on temperature, which can be explained with zero mass flux condition at the wall.
6. The nanoparticles are concentrated near the wall of cone or wedge and the negative value of φ at the wall $(\eta = 0)$, illustrate that concentration of nanoparticles at surface is lower than ambient value of concentration.
7. The effect of magnetic parameter *M*, thermal radiation parameter *Rd*, thermophoresis parameter *Nt* and volume fraction ϕ is to increase the concentration when fluid moves towards ambient field whereas opposite trend is observed for parameters *s*, *Nb*, *Sc* and *Kr*.
8. The drag force at the surface can be reduced with increasing the values of mixed convection parameter λ but it increases with increasing magnetic parameter and volume fraction.
9. The heat transfer rate at the wall of cone or wedge can be increased by increasing thermal radiation, parameter *s* and γ_t.

Author Contributions

S.K. Rawat: Presented the idea, developed the model, investigated the problem, performed the computations, verified the numerical methods and results, discussed the results and wrote original draft of the paper. H. Upreti: Developed the model, performed the computations, discussed the results and helped in writing the original draft. M. Kumar: Developed

the model, supervised the whole process, discussed the results, reviewed and edited the draft of the paper.

Acknowledgments

The authors want to express sincere thanks to anonymous reviewers for their helpful feedback and comments to improve manuscript content.

Conflict of Interest

The authors declared no potential conflicts of interest with respect to the research, authorship and publication of this article.

Funding

Research was supported by UGC (F. No. 16-6 (Dec. 2017)/2018 (NET/CSIR)), Government of India and gratefully acknowledged by the first author.

Nomenclature

a, A, B	Constant
B_o	Magnetic field
C	Concentration of the fluid
C_f	Skin friction coefficient
C_0, D	Constant
D_B	Brownian diffusion coefficient
D_T	Thermophoretic diffusion coefficient
E, F	Constant
f'	Dimensionless velocity
Gr_x	Local Grashof number
g	Acceleration due to gravity
$\boldsymbol{j}$	Mass flux
k	Thermal conductivity
K_0	Reaction rate
Kr	Chemical reaction rate parameter
k^*	Mean absorption coefficient
l	Characteristic length
M	Magnetic parameter
Nb	Brownian motion parameter
Nr	Buoyancy ratio parameter
Nt	Thermophoretic parameter
Nu_x	Local Nusselt number
Pr	Prandtl number
q_r	Radiation heat flux
$\boldsymbol{q}$	Heat flux
r	Radius of cone
Re_x	Local Reynolds number
Rd	Thermal radiation parameter
s	Wall temperature related parameter
Sc	Schmidt number
T	Temperature of the fluid
u	Velocity component in x- direction
v	Velocity component in y- direction
$\mathbf{v}$	Velocity
x, y	Cartesian coordinate system

Greek symbols

α	Half angle of cone or wedge
β	Thermal expansion coefficient
γ_t	Thermal relaxation time parameter
γ_c	Solutal relaxation time parameter
η	Similarity variable
Θ	Dimensionless temperature
λ	Mixed convection parameter
μ	Dynamic viscosity
ν	Kinematic viscosity
ρ	Effective density
ρc_p	Heat capacity
σ	Electrical conductivity
τ	Ratio of the effective heat capacity of nanomaterial/base fluid
τ_t	Heat flux relaxation time
τ_c	Mass flux relaxation time
σ^*	Stefan-Boltzmann constant
φ	Dimensionless concentration
ϕ	Volume fraction of nanoparticle

Superscript

'	Derivative w.r.t η

Subscript

f	Base fluid
nf	Nanofluid
p	Solid particle
w	Wall
∞	Ambient condition

References

[1] Choi, S.U.S., Enhancing Thermal Conductivity of Fluids with Nanoparticles, Developments and Applications of Non-Newtonian Flows, *ASME J. Heat Transfer*, 66, 1995, 99–105.

[2] Hady, F.M., Ibrahim, F.S., Abdel-Gaied, S.M., Eid, M.R., Effect of heat generation/absorption on natural convective boundary-layer flow from a vertical cone embedded in a porous medium filled with a non-Newtonian nanofluid, *International Communications in Heat and Mass Transfer*, 38(10), 2011, 1414-1420.

[3] Alsaedi, A., Awais, M., Hayat, T., Effects of heat generation/absorption on stagnation point flow of nanofluid over a surface with convective boundary conditions, *Communications in Nonlinear Science and Numerical Simulation*, 17(11), 2012,

4210-4223.
[4] Jalilpour, B., Jafarmadar, S., Ganji, D.D., Shotorban, A.B., Taghavifar, H., Heat generation/absorption on MHD stagnation flow of nanofluid towards a porous stretching sheet with prescribed surface heat flux, *Journal of Molecular Liquids*, 195, 2014, 194-204.
[5] Pal, D. and Mandal, G., Mixed convection–radiation on stagnation-point flow of nanofluids over a stretching/shrinking sheet in a porous medium with heat generation and viscous dissipation, *Journal of Petroleum Science and Engineering*, 126, 2015, 16-25.
[6] Rawat, S.K., Pandey, A.K. and Kumar, M., Effects of chemical reaction and slip in the boundary layer of MHD nanofluid flow through a semi-infinite stretching sheet with thermophoresis and Brownian motion: the lie group analysis, *Nanoscience and Technology: An International Journal*, 9(1), 2018, 47-68.
[7] Rawat, S.K., Mishra, A., Kumar, M., Numerical study of thermal radiation and suction effects on copper and silver water nanofluids past a vertical Riga plate, *Multidiscipline Modeling in Materials and Structures*, 15(4), 2019, 714-736.
[8] Khan, W.A., Rashad, A.M., Abdou, M.M.M., Tlili, I., Natural bioconvection flow of a nanofluid containing gyrotactic microorganisms about a truncated cone, *European Journal of Mechanics-B/Fluids*, 75, 2019, 133-142.
[9] Patil, P.M., Shashikant, A. and Hiremath, P.S., Diffusion of liquid hydrogen and oxygen in nonlinear mixed convection nanofluid flow over vertical cone, *International Journal of Hydrogen Energy*, 44(31), 2019, 17061-17071.
[10] Fourier, J.B.J., *Théorie analytique de la chaleur: Paris*, Académie des Sciences, 1822.
[11] Cattaneo, C., Sulla conduzione del calore, *Atti Sem. Mat. Fis. Univ. Modena*, 3, 1948, 83-101.
[12] Christov, C.I., On frame indifferent formulation of the Maxwell–Cattaneo model of finite-speed heat conduction. *Mechanics Research Communications*, 36(4), 2009, 481-486.
[13] Upadhya, S.M., Raju, C.S.K., Saleem, S., Nonlinear unsteady convection on micro and nanofluids with Cattaneo-Christov heat flux, *Results in Physics*, 9, 2018, 779-786.
[14] Alamri, S.Z., Khan, A.A., Azeez, M. and Ellahi, R., Effects of mass transfer on MHD second grade fluid towards stretching cylinder: a novel perspective of Cattaneo–Christov heat flux model, *Physics Letters A*, 383(2-3), 2019, 276-281.
[15] Rawat, S.K., Upreti, H., Kumar, M, Thermally stratified nanofluid flow over porous surface cone with Cattaneo–Christov heat flux approach and heat generation (or) absorption, *SN Appl. Sci.* 2, 302, 2020.
[16] Hayat, T., Khan, M.I., Farooq, M., Alsaedi, A., Waqas, M., Yasmeen, T., Impact of Cattaneo–Christov heat flux model in flow of variable thermal conductivity fluid over a variable thicked surface, *International Journal of Heat and Mass Transfer*, 99, 2016, 702-710.
[17] Han, S., Zheng, L., Li, C., Zhang, X., Coupled flow and heat transfer in viscoelastic fluid with Cattaneo–Christov heat flux model, *Applied Mathematics Letters*, 38, 2014, 87-93.
18] Hayat, T., Farooq, M., Alsaedi, A., Al-Solamy, F., Impact of Cattaneo-Christov heat flux in the flow over a stretching sheet with variable thickness, *AIP Advances*, *5*(8), 2015, 087159.
[19] Mabood, F., Khan, W.A, Analytical study for unsteady nanofluid MHD Flow impinging on heated stretching sheet, *Journal of Molecular Liquids*, 219, 2016, 216-223.
[20] Sheikholeslami, M., Ganji, D.D., Javed, M.Y., Ellahi, R., Effect of thermal radiation on magnetohydrodynamics nanofluid flow and heat transfer by means of two phase model, *Journal of Magnetism and Magnetic Materials*, 374, 2015, 36–43.
[21] Pal, D., Mandal, G., Vajravelu, K., Flow and heat transfer of nanofluids at a stagnation point flow over a stretching/shrinking surface in a porous medium with thermal radiation, *Applied Mathematics and Computation*, 238**,** 2014, 208–224.
[22] Hamid, M., Usman, M., Zubair, T., Haq, R.U., Wang, W., Shape effects of MoS2 nanoparticles on rotating flow of nanofluid along a stretching surface with variable thermal conductivity: A Galerkin approach, *International Journal of Heat and Mass Transfer*, 124, 2018, 706-714.
[23] Atif, S.M., Hussain, S., Sagheer, M., Heat and mass transfer analysis of time-dependent tangent hyperbolic nanofluid flow past a wedge, *Physics Letters A*, 383(11), 2019, 1187-1198.
[24] Zangooee, M.R., Hosseinzadeh, K., Ganji, D.D., Hydrothermal analysis of MHD nanofluid (TiO2-GO) flow between two radiative stretchable rotating disks using AGM, *Case Studies in Thermal Engineering*, 14, 2019, 100460.
[25] Aleem, M., Asjad, M.I., Shaheen, A., Khan, I., MHD Influence on different water based nanofluids (TiO2, Al2O3, CuO) in porous medium with chemical reaction and newtonian heating, *Chaos, Solitons & Fractals*, 130, 2020, 109437.
[26] Krishna, M.V., Chamkha, A.J., Hall and ion slip effects on MHD Rotating Boundary layer flow of Nanofluid past an infinite vertical plate Embedded in a Porous medium, *Results in Physics*, 2019, 102652.
[27] Gholinia, M., Hoseini, M.E., Gholinia, S., A numerical investigation of free convection MHD flow of Walters-B nanofluid over an inclined stretching sheet under the impact of Joule heating, *Thermal Science and Engineering Progress*, 11, 2019, 272-282.
[28] Souayeh, B., Reddy, M.G., Sreenivasulu, P., Poornima, T., Rahimi-Gorji, M., Alarifi, I.M., Comparative analysis on non-linear radiative heat transfer on MHD Casson nanofluid past a thin needle, *Journal of Molecular Liquids*, 284, 2019, 163-174.
[29] Singh, K., Rawat, S.K., Kumar, M., Heat and mass transfer on squeezing unsteady MHD nanofluid flow between parallel plates with slip velocity effect, *Journal of Nanoscience*, 2016, Article ID 9708562, 11 pages.
[30] Singh, J., Mahabaleshwar, U.S., Bognár, G., Mass transpiration in nonlinear MHD flow Due to porous Stretching Sheet, *Scientific Reports*, 9(1), 2019, 1-15.

[31] Upreti, H., Rawat, S.K., Kumar, M., Radiation and non-uniform heat sink/source effects on 2D MHD flow of CNTs-H2O nanofluid over a flat porous plate, *Multidiscipline Modeling in Materials and Structures*, 2019. https://doi.org/10.1108/MMMS-08-2019-0153
[32] Dhlamini, M., Kameswaran, P.K., Sibanda, P., Motsa, S., Mondal, H., Activation energy and binary chemical reaction effects in mixed convective nanofluid flow with convective boundary conditions, *Journal of Computational Design and Engineering*, 6(2), 2019, 149-158.
[33] Rasool, G., Zhang, T., Characteristics of chemical reaction and convective boundary conditions in Powell-Eyring nanofluid flow along a radiative Riga plate, *Heliyon*, 5(4), 2019, e01479.
[34] Khan, M.I., Alsaedi, A., Qayyum, S., Hayat, T., Khan, M.I., Entropy generation optimization in flow of Prandtl–Eyring nanofluid with binary chemical reaction and Arrhenius activation energy, *Colloids and Surfaces A: Physicochemical and Engineering Aspects*, 570, 2019, 117-126.
[35] Khan, N.S., Kumam, P., Thounthong, P., Second law analysis with effects of Arrhenius activation energy and binary chemical reaction on nanofluid flow, *Scientific Reports*, 10(1), 2020, 1-16.
[36] Yadav, D., Impact of chemical reaction on the convective heat transport in nanofluid occupying in porous enclosures: A realistic approach, *International Journal of Mechanical Sciences*, 157, 2019, 357-373.
[37] Tiwari, R.K., Das, M.K., Heat transfer augmentation in a two-sided lid-driven differentially heated square cavity utilizing nanofluids, *International Journal of Heat and Mass Transfer*, 50(9-10), 2007, 2002-2018.
[38] Buongiorno, J., Convective transport in nanofluids, *Journal of Heat Transfer*, 128(3), 2006, 240-250.
[39] Noor, A., Nazar, R., Jafar, K., Pop, I., Boundary-layer flow and heat transfer of nanofluids over a permeable moving surface in the presence of a coflowing fluid, *Advances in Mechanical Engineering*, 6, 2014, 521236.
[40] Rana, P., Dhanai, R., Kumar, L., MHD slip flow and heat transfer of Al2O3-water nanofluid over a horizontal shrinking cylinder using Buongiorno's model: Effect of nanolayer and nanoparticle diameter, *Advanced Powder Technology*, 28(7), 2017, 1727-1738.
[41] Rana, P., Shukla, N., Bég, O.A., Bhardwaj, A., Lie group analysis of nanofluid slip flow with Stefan Blowing effect via modified Buongiorno's Model: entropy generation analysis, *Differential Equations and Dynamical Systems*, 2019, 1-18.
[42] Malvandi, A., Moshizi, S.A., Soltani, E.G., Ganji, D.D., Modified Buongiorno's model for fully developed mixed convection flow of nanofluids in a vertical annular pipe, *Computers & Fluids*, 89, 2014, 124-132.
[43] Alhashash, A., Natural convection of Nanoliquid from a Cylinder in Square Porous Enclosure using Buongiorno's Two-phase Model, *Scientific Reports*, 10(1), 2020, 1-12.
[44] Hayat, T., Aziz, A., Muhammad, T., Alsaedi, A., Model and comparative study for flow of viscoelastic nanofluids with Cattaneo-Christov double diffusion, *PloS One*, 12(1), 2017, e0168824.
[45] Hayat, T., Muhammad, T., Alsaedi, A., Ahmad, B., Three-dimensional flow of nanofluid with Cattaneo–Christov double diffusion, *Results in Physics*, 6, 2016, 897-903.
[46] Ijaz, M., Ayub, M., Activation energy and dual stratification effects for Walter-B fluid flow in view of Cattaneo-Christov double diffusion, *Heliyon*, 5(6), 2019, e01815.
[47] Khan, W.A., Khan, M., Alshomrani, A.S., Impact of chemical processes on 3D Burgers fluid utilizing Cattaneo-Christov double-diffusion: applications of non-Fourier's heat and non-Fick's mass flux models, *Journal of Molecular Liquids*, 223, 2016, 1039-1047.
[48] Muhammad, N., Nadeem, S., Mustafa, T., Squeezed flow of a nanofluid with Cattaneo–Christov heat and mass fluxes, *Results in Physics*, 7, 2017, 862-869.
[49] Sui, J., Zheng, L., Zhang, X., Boundary layer heat and mass transfer with Cattaneo–Christov double-diffusion in upper-convected Maxwell nanofluid past a stretching sheet with slip velocity, *International Journal of Thermal Sciences*, 104, 2016, 461-468.
[50] Kuznetsov, A.V., Nield, D.A., Natural convective boundary-layer flow of a nanofluid past a vertical plate: A revised model, *International Journal of Thermal Sciences*, 77, 2014, 126-129.
[51] Kuznetsov, A.V., Nield, D.A., The Cheng–Minkowycz problem for natural convective boundary layer flow in a porous medium saturated by a nanofluid: a revised model, *International Journal of Heat and Mass Transfer*, 65, 2013, 682-685.
[52] Lu, D., Ramzan, M., ul Huda, N., Chung, J.D., Farooq, U., Nonlinear radiation effect on MHD Carreau nanofluid flow over a radially stretching surface with zero mass flux at the surface, *Scientific Reports*, 8(1), 2018, 1-17.
[53] Rauf, A., Shehzad, S.A., Hayat, T., Meraj, M.A., Alsaedi, A., MHD stagnation point flow of micro nanofluid towards a shrinking sheet with convective and zero mass flux conditions, *Bulletin of the Polish Academy of Sciences Technical Sciences*, 65(2), 2017, 155-162.
[54] Kumar, K.A., Sugunamma, V., Sandeep, N., Mustafa, M.T., Simultaneous solutions for first order and second order slips on micropolar fluid flow across a convective surface in the presence of Lorentz force and variable heat source/sink, *Scientific Reports*, 9(1), 2019, 1-14.
[55] Vajravelu, K., Nayfeh, J., Hydromagnetic convection at a cone and a wedge, *International Communications in Heat and Mass Transfer*, 19(5), 1992, 701-710.
[56] Sandeep, N., Reddy, M.G., Heat transfer of nonlinear radiative magnetohydrodynamic Cu-water nanofluid flow over two different geometries, *Journal of Molecular Liquids*, 225, 2017, 87-94.

How to cite this article: S.K. Rawat, H. Upreti, M. Kumar, Comparative Study of Mixed Convective MHD Cu-Water Nanofluid Flow over a Cone and Wedge using Modified Buongiorno's Model in Presence of Thermal Radiation and Chemical Reaction via Cattaneo-Christov Double Diffusion Model, *J. Appl. Comput. Mech.*, 7(3), 2021, 1383–1402. https://doi.org/10.22055/JACM.2020.32143.1975